Wide-energy-range electron characterization of the Aug 2018 geomagnetic storm: CSES-01 contribution

A. Parmentier[1,*], M. Martucci[2], A. Sotgiu[1], L. Carfora[1,2], M. Piersanti[1], S. Bartocci[1], R. Battiston[3,4], W. J. Burger[3], D. Campana[5], G. Castellini[6], L. Conti[1,7], A. Contin[8,9], C. De Donato[1], F. De Persio[1], C. De Santis[1], P.Diego[10], F. M. Follega[3,4], R. Iuppa[3,4], I. Lazzizzera[3,4], G. Masciantonio[1], M. Mergé[1], G. Osteria[5], F. Palma[1], F. Palmonari[8,9], B. Panico[5], F. Perfetto[5], P. Picozza[1,2], M. Pozzato[9], I. Rashevskaya[3], E. Ricci[3,4], M. Ricci[11], S. Ricciarini[6], X. Shen [12], V. Scotti[5,13], R. Sparvoli[1,2], B. Spataro[11], P. Ubertini[10], V. Vitale[1], Z. Zeren[12], S. Zoffoli[14], P. Zuccon[3,4]

[1]INFN - Division of Roma Tor Vergata, via della Ricerca Scientifica 1, 00133, Rome, Italy
[2]University of Roma Tor Vergata, Dept. of Physics, via della Ricerca Scientifica 1, 00133, Rome, Italy
[3]INFN-TIFPA, via Sommarive 14, 38123, Povo (TN), Italy
[4]University of Trento, via Sommarive 14, 38123, Povo (TN), Italy
[5]INFN - Division of Naples, via Cinthia, 80126, Naples, Italy
[6]IFAC - CNR, via Madonna del Piano 10, 50019, Sesto Fiorentino (FI), Italy
[7]Uninettuno University, c.so Vittorio Emanuele II 39, 00186, Rome, Italy
[8]University of Bologna, v.le Berti Pichat 6/2, Bologna, Italy
[9]INFN - Division of Bologna, v.le Berti Pichat 6/2, Bologna, Italy
[10]INAF-IAPS, via Fosso del cavaliere 100, 00133, Rome, Italy
[11]INFN - LNF, via E. Fermi 40, 00044, Frascati (RM), Italy
[12]Institute of Crustal Dynamics, CEA, 1 Anningzhuang Rd, Haidian District, Beijing, China
[13]University of Naples "Federico II", via Cinthia 21, 80126, Naples, Italy
[14]Italian Space Agency, via del Politecnico, 00133, Rome, Italy

Key Points:

- CSES-01 data permit an extended characterization of the storm-time magnetospheric e^- rearrangement across the range from a few hundreds keV to the relativistic region
- Striking consistence of data with measurements from concurrent missions reveals CSES-01's excellent capabilities in the field of Space Weather

Corresponding author: Alexandra Parmentier, alexandra.parmentier@roma2.infn.it

Abstract

On Aug 25, 2018, a G3-class geomagnetic storm, driven by a slow coronal mass ejection from the Sun, impacted the Earth's magnetosphere causing a transient rearrangement of the charged-particle environment around the planet, which was clearly detected by the entire suite of detectors on board the CSES-01 satellite. In this work, a systematic characterization of the magnetospheric response to the disturbance is reported on the base of complementary electron-flux measurements from the high-energy particle detectors (HEPP-L/H, and HEPD) embarked on CSES-01. CSES-01 results are compared to homologous data from active ground-based and in-orbit instrumentation, and assessed to fit established scenarios in mainstream space-weather scientific literature.

1 Introduction

In their most typical configuration, the Earth's radiation belts (RBs) consist of an outer portion (ORB), more dynamic and basically containing high-energy electrons (Turner et al., 2019) and ring-current ions (Keika et al., 2013), and a more stable inner part (IRB), which mainly accommodates high-energy protons from albedo-neutron processes (CRAND) (Selesnick et al., 2007), as well as $O(1)$ MeV electrons (Fennell et al., 2015). The two belts are usually separated by a narrow slot region (SR), which, in quiet conditions, is tipically located between $L \sim 2$ and $L \sim 3$. The SR is mostly devoid of electrons due to the balance between inward radial diffusion from a source located in the ORB and resonant pitch-angle scattering (Lyons et al., 1972). L is the L-shell parameter, which describes the set of magnetic field lines crossing the Earth's magnetic equator at a number of Earth radii corresponding to the value of L itself.

The marked variability of MeV electron fluxes in the ORB (Goldstein et al., 2016; Baker et al., 2016, 2019; Katsavrias et al., 2019) on a short a time scale of a few hours in geomagnetically disturbed periods - occasionally of $O(1)$MeV electrons in the IRB and during slot-filling events (Turner et al., 2015; Reeves et al., 2016; Turner et al., 2017) - is a well-established topic that is raising increasing scientific interest due to the global economic impact of space weather on technological infrastructures (Eastwood et al., 2018; Piersanti & Carter, 2019) and radiation risks posed to space missions (Dietze et al., 2013). This has been highlighted by the Committee on Space Research (COSPAR) and the ILWS Steering Committee, which have recently commissioned a strategic assessment on the science of Space Weather (Schrijver et al., 2015).

Regarding the electron flux variations in the ORB, in addition to adiabatic effects caused by inflation of drift orbits in response to diamagnetic effect of storm-time ring-current buildup (McIlwain, 1966), two major acceleration mechanisms are usually at play: 1) short-timescale local "heating", whose origin is mainly the resonating interaction of low-frequency chorus waves with "seed" electron populations (several tens to a few hundred keV) provided by substorm plasma injections from magnetotail and enhanced global convection (Thorne et al., 2013; Jaynes et al., 2015); and 2) radial diffusion triggered by drift resonance between trapped particles and low-frequency oscillations of the magnetosphere driven by a variety of phenomena (Claudepierre et al., 2008; Zong et al., 2009; Piersanti et al., 2012; James et al., 2013). Flux dropouts of relativistic electrons are commonly observed during the main phase of a geomagnetic storm, due to the so-called, adiabatic "Dst effect" (Ganushkina et al., 2017), as well as true particle losses occurring either in the ionosphere or the magnetopause as a result of wave-particle interactions that violate the adiabatic invariants in stretched portions of the magnetotail (Schulz & Lanzerotti, 1974; Turner et al., 2012; Ukhorskiy et al., 2015). The substorm processes can lead to prompt energization of highly relativistic electrons (> 5 MeV) in the region outside the plasmapause (Foster et al., 2014).

On the other hand, events known as sudden particle enhancements at low L shells (SPELLS) (Turner et al., 2017) usually witness important injections of hundreds-keV electrons into the IRB and SR during major geomagnetic disturbances (Reeves et al., 2016), with

inward radial diffusion successfully competing with pitch-angle scattering by plasmaspheric hiss, magnetosonic waves, and VLF transmitter waves in the slot (Ma et al., 2017).

During short-term solar events, Solar Energetic Particles (SEPs), can occasionally reach the Earth even in a few minutes (Adriani et al., 2015), after acceleration in the solar corona and injection into the interplanetary space. SEPs exceeding the > 500 MeV threshold are able to penetrate into the Earth's atmosphere, where they initiate atmospheric cascades, which can be registered by ground-level detectors (Andriopoulou et al., 2011), causing phenomena named Ground Level Enhancements, or GLEs (Adriani et al., 2015; Asvestari et al., 2017; Piersanti et al., 2017).

Solar flares and CMEs are more frequent during maximum phases of solar activity, but extreme events can take place during quiet periods as well (Kay et al., 2019). The current 24^{th} solar cycle keeps winding down, and has been predicted to reach solar minimum in late 2019 or 2020 (Pesnell, 2008). Cycle 25 is slowly coming to life as highligthed by the inverse magnetic polarity (Hale et al., 1919) of sunspot AR2744 emerged in solar southern hemisphere in July 2019 (`https://sdo.gsfc.nasa.gov/data/`). Nonetheless, cycle 24 has been producing significant events, such as the slow interplanetary coronal mass ejection (ICME) that, just after the end of CSES-01 commissioning phase, impacted the Earth's magnetosphere on Aug 25, 2018, following the eruption of a modest solar filament on Aug 20 (Piersanti, 2019).

In this paper, we analyze the magnetospheric electron response to the strong geomagnetic storm triggered by the Aug 2018 ICME, with special focus on the re-arrangement in L shell of RB electrons, using particle data collected by the China Seismo-Electromagnetic Satellite (CSES-01, Fig. 1), which are compared to homologous observations by concurrent missions. CSES-01 was launched in Feb 2018 to reach a nearly-polar, Sun-synchronous Low Earth Orbit (LEO) at an altitude of about 507 km for an expected lifespan of at least 5 years (Shen et al., 2018). Though conceived as a mission to primarily investigate possible correlations between e.m. emissions induced by seismic/volcanic/anthropogenic activity and short-term perturbations of the Earth's iono/magnetosphere (Yan et al., 2018; Zhang et al., 2018), CSES-01 is equally well suited to monitor variations in the Earth-Sun interaction under quiet conditions and during geomagnetic-storm transients through detection of both particle precipitation and magnetospheric entrapment, which is especially important in a period when many key space-weather instruments are well beyond the end of their scheduled lifetimes.

Monitored electron energies spanned the wide range from a few hundred keV to a dozen MeV, thanks to the combined detection by the two particle instruments belonging to the High Energy Particle Package (HEPP) (Li et al., 2019), and the High Energy Particle Detector (HEPD) (Picozza et al., 2019). In addition, $E > 150$ MeV galactic protons at high latitudes were monitored by HEPD.

The paper is organized as follows. After Introduction, Section 2 summarizes CSES-01 data types used in this work, as well as complementary public data from other in-flight and ground-based active missions. Section 3 makes a description of major solar and geomagnetic characteristics of the Aug 2018 storm. Section 4 reports an overview of electron fluxes observed by the entire suite of CSES-01 particle detectors during the disturbance, with comparison to concurrent data from homologous detectors on board NOAA-15/POES and RBSP-A. Finally, Section 5 presents data discussion and a summary, framing CSES-01 observations within the current status of Space-Weather studies.

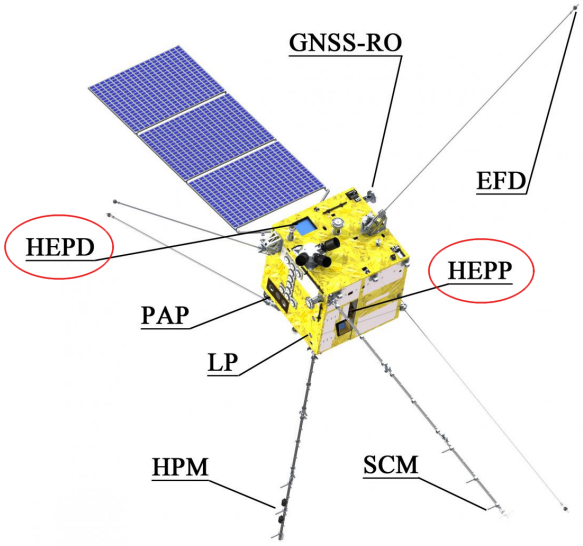

Figure 1. In-orbit configuration of CSES-01. The positions of HEPD (zenith pointing) and HEPP-L/H are marked in red.

2 Datasets

2.1 The particle-detector suite on board CSES-01

HEPP, developed at the Institute of High Energy Physics (IHEP) of the Chinese Academy of Sciences (CAS), consists of two charged-particle detectors (HEPP-L/H) and one solar X-ray monitor (HEPP-X) described in detail in (Li et al., 2019). As to electron detection, HEPP-L and HEPP-H span the energy ranges 0.1-3.0 MeV and 1.5-50.0 MeV, respectively. HEPP electron data are provided with time resolution at 1 s.

The HEPD detector was built by the Italian LIMADOU Collaboration. A detailed description of the apparatus can be found in (Picozza et al., 2019). HEPD is aimed to detect electrons in the energy range between 3 and 100 MeV, and protons between 30 and 200 MeV, as well as light nuclei in the $O(100)$ MeV energy window. HEPD particle data used in this work are event-based, *i.e.*, higher-level information (such as energy) is reconstructed from single triggers.

2.2 Additional data

In support to our storm-time particle observations, additional experimental data from both satellite and ground-based missions have been used within the text.

The CDAWeb dataset (`https://cdaweb.sci.gsfc.nasa.gov/`) and the World Data Center for Geomagnetism of Kyoto (`http://wdc.kugi.kyoto-u.ac.jp/`) were gleaned from in order to retrieve interplanetary magnetic field (IMF) parameters, as well as indices of geomagnetic activity. As reported in detail in the Acknowledgements Section, additional electron, proton, neutron, and X-ray data were recovered from NOAA Space Weather Prediction Center (`https://www.swpc.noaa.gov/`), NOAA National Geophysical Data Center (`https://ngdc.noaa.gov/ngdc.html`), Real-Time Neutron Monitor Database (`www.nmdb.eu`), and RBSP-ECT Science Operations and Data Center (`https://www.rbsp-ect.lanl.gov/rbsp_ect.php`, and `https://rbspgway.jhuapl.edu`).

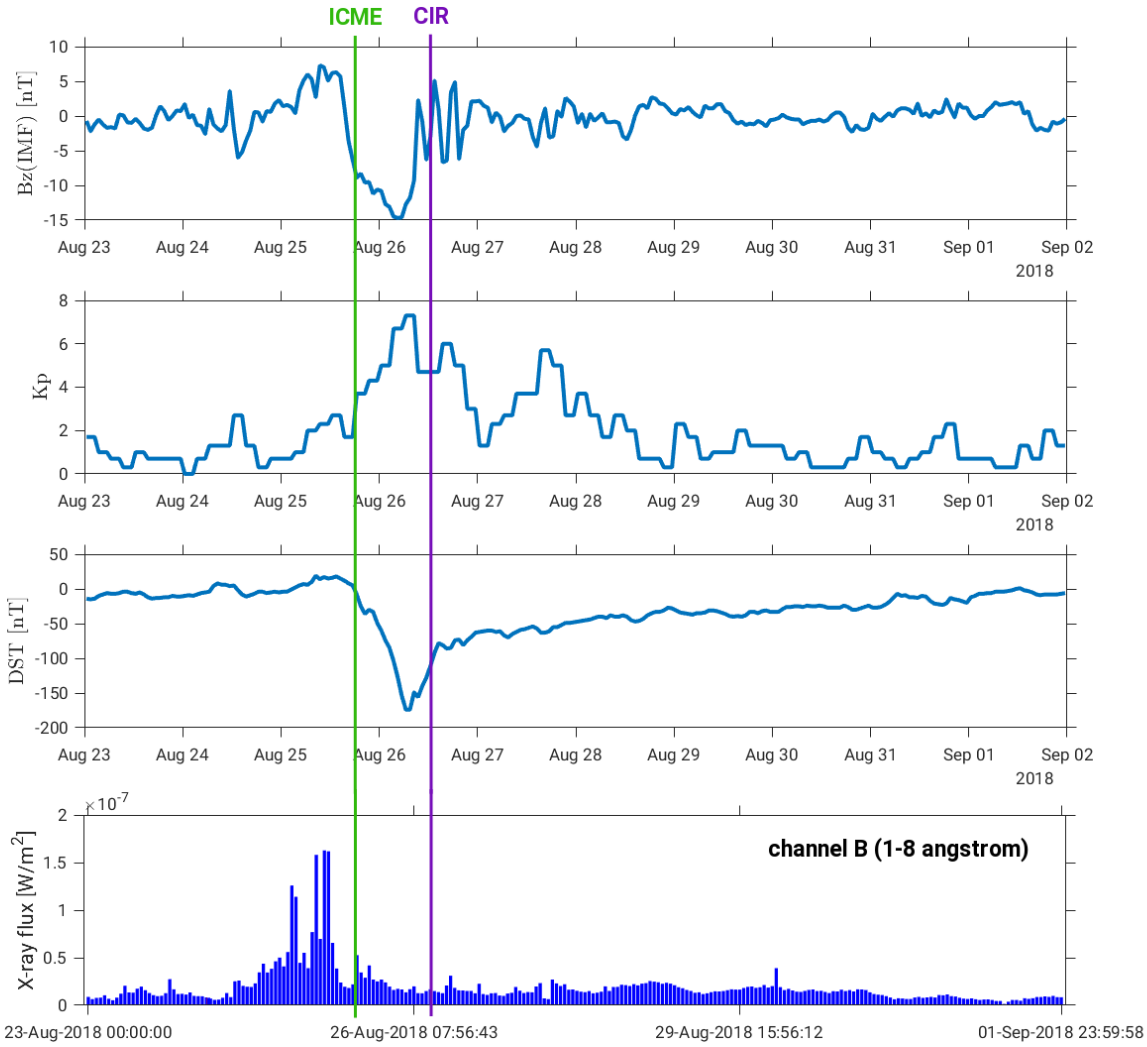

Figure 2. From top to bottom, storm-time evolution of z-component of the IMF, Kp index, Dst index, and GOES-15 X-ray flux (channel B: 1-8 Å), respectively. Vertical colored lines mark the arrival of: ICME (green) and co-rotating interaction region, CIR (violet).

3 The Aug 2018 storm

The Aug 2018 ICME, though labeled as "slow"(Piersanti, 2019; Iju et al., 2013), was able to trigger a strong geomagnetic storm (G3 class), with persistent southward z component (down to ~ -20 nT) of the interplanetary magnetic field (IMF), B_z^{IMF}; Kp index reaching level 7 on Aug 26; and Dst index reaching ~ -180 nT. The ICME was also immediately followed by the production of a co-rotating interaction region (CIR) in the interplanetary space, which made B_z^{IMF} turn negative again (Fig. 2).

The solar X-ray flux remained below B level ($< \frac{10^{-7}W}{m^2}$), with the exception of Aug 25, when a series of low B flares were produced, as detected by GOES-15 X-ray monitor in the 1-8 Å channel (Fig. 2).

The storm was marked by high auroral activity ($AE_{max} > 2100$ nT) till mid Aug 28, with significant loading of the magnetotail current during main phase (max abs value of

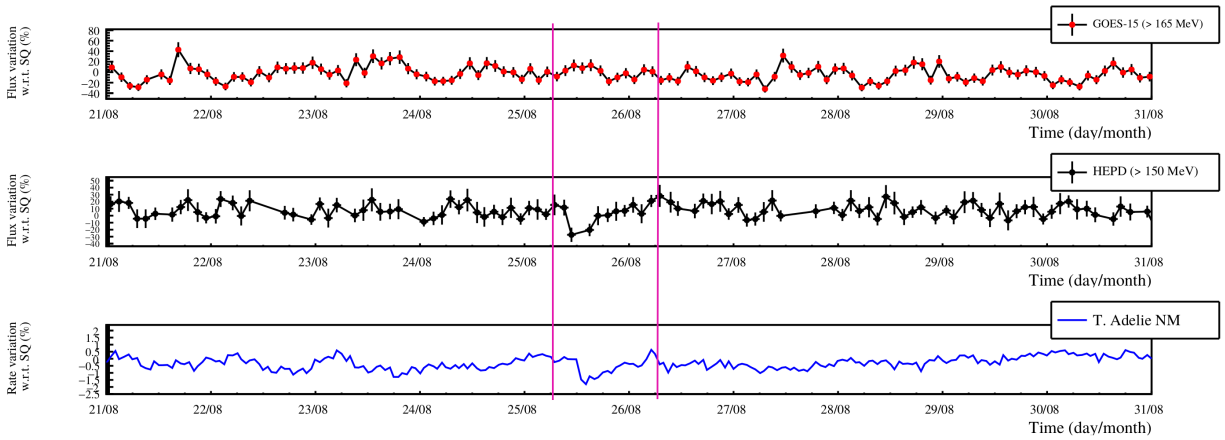

Figure 3. Percent flux variation of galactic-proton population as a function of Coordinated Universal Time (UTC) with respect to the quiet period of Aug 8-12, 2018, observed by 3 instruments. From top to bottom: $>$ 165 MeV protons detected by GOES-15, $>$ 150 MeV protons detected by HEPD on board CSES-01 (3-hr binning), and secondary neutrons from TERA ADELIE Neutron Monitor, respectively.
The South Atlantic Anomaly (SAA) is excluded from HEPD data for consistence with electron data presented in Section 4.
No evident solar particle injection has been detected either in space or on ground. Nevertheless, small changes in magnetic field configuration, due to storm arrival, are present in the time profiles of HEPD and TERA ADELIE, causing a small depletion/peak structure in the time interval (enclosed between magenta lines) roughly corresponding to the main phase of the storm.

westward component AL$\sim$ 2000 nT) and prolonged substorm activity during recovery (see `http://wdc.kugi.kyoto-u.ac.jp/` for quick-look data).

As reported by NOAA Space Environment Services Center (`https://umbra.nascom.nasa.gov/SEP/`), no SEPs affected the Earth environment during the storm. Accordingly, no significant solar-proton injection was registered, resulting in negligible galactic proton flux disturbances in comparison to a quiet (Kauristie et al., 2017) revisit interval of early Aug 2018 (Fig. 3), as assessed by multiple ground-based and satellite instruments, including HEPD. It is worth remarking here that the depletion/peak structure, observed in close proximity to the main phase of the storm by both TERA ADELIE neutron monitor on ground and HEPD from space, is due to a magnetic disturbance triggered by the impinging storm, which produces small changes in the configuration of cutoff rigidities. Indeed, cutoff rigidities are influenced by geomagnetic activity, with typical equatorward drift of corresponding cutoff latitudes (*i.e.*, the lowest geomagnetic latitudes at which a charged cosmic-ray particle of specific energy can penetrate the Earth's magnetic field) in case of southward rotation of B_z^{IMF} (Adriani et al., 2016).

HEPD galactic protons of energy larger than 150 MeV were selected at Altitude Adjusted Corrected GeoMagnetic (AACGM) latitudes $>$ $|75°|$ through formalization of the internal geomagnetic field source by the 12^{th} generation of the International Geomagnetic Reference Field (IGRF12) model (Thébault et al., 2015). Indeed, CSES-01 orbit allows HEPD to be sensitive to galactic protons only at very polar latitudes, *i.e.*, close to the regions monitored by TERA ADELIE, which makes their observations very similar in shape to each other, but not in magnitude (HEPD operates at an altitude of $\sim$ 500 km).

4 Storm-time electron dynamics in Aug 2018

Fig. 4 shows 2D maps - in UTC and L shell - of storm-time electron flux variations detected by HEPP-L/H and HEPD over several energy sub-ranges included in the 0.2-11.0 MeV range, with geomagnetic latitudes and L shells modeled by means of the IGRF12 model. Percent flux variations are computed with respect to a close quiet background ($100 \times \frac{f-f_{SQ}}{f_{SQ}}$, with f_{SQ} the background flux) including an entire CSES-01 revisit time in order to emphasize flux dropouts from ring-current enhancement at storm peak. Data shown in Fig. 4 represent a quick and comprehensive overview of electron rearrangement in L shell across the various storm phases, with changing features that strictly depend on the energy range considered (extensively discussed in Section 5).

Specifically, HEPP-L and HEPP-H have been used to cover the 0.2-5 MeV energy range. Any HEPP map has 6-hr time binning and L resolution of 0.2 R_E. Here, only night-side semi-orbits have been selected in order to better capture storm-time injections of plasma from the neutral sheet of the magnetotail. Indeed, a southward IMF induces the conversion of closed magnetic-field lines of the Earth to an open topology by so-called "reconnection" (Fig. 5). The flow of the solar wind stretches open field lines antisunwards to form the magnetotail lobes, and eventually reconnection in the neutral sheet triggers the closure of open lines and their "traveling back" to the day side to complete (and repeat) the cycle, as first described by Dungey (Dungey, 1961).

On the other hand, the HEPD detector has been used to monitor the energy range above 5 MeV and within 11 MeV. Here, at least two different points must be taken into account. First, a strong decrease (by orders of magnitude) in intensity of flux variations is usually observed at increasing particle energy (Turner et al., 2015), with electrons of the highest energies experiencing prolonged recovery (up to several weeks) especially during storms marked by flux enhancements (Zhao et al., 2019; Katsavrias et al., 2019). In addition, HEPD can be configured with different trigger conditions (Ambrosi et al., 2020). The trigger configuration implemented for the present data collection was the one labeled as T&P1&P2, which corresponds to event acquisition and processing only when the release of energy in the trigger plane (T), and the first two planes of the calorimeter (P1, P2), is above a predefined threshold. In this configuration, 100% counting efficiency is obtained for electron energies larger than ~ 8 MeV, even though triggering is still possible at lower energies, though with very small efficiency that decrease to 0 at ~ 3 MeV (50% efficiency at ~ 5 MeV). For all these reasons, HEPD maps have been divided by geographical hemisphere instead of day/night side. Correspondingly, in any map, time binning and L resolution have been enlarged to 48 hours and ~ 0.3 R_E, respectively, for the sake of statistical stability.

For better appreciating radiation-belt rearrangement over the < 650 keV and relativistic energy ranges, 1D L distributions of flux variations for pre-main and main phases, as well as for a bunch of single days falling in recovery phase, are reported in Figs. 6 and 7, with comparison to homologous flux determinations by other active missions (NOAA-15/POES and RBSP-A/ECT) with the purpose of framing CSES-01 observations within the *corpus* of concurrent experimental data.

The adiabatic buildup of the ring current, whose diamagnetic effects induce the stretching of the night-side magnetic field and the pushing of electron drift orbits outwards, has been monitored using $\sim$ 39 keV protons detected by MEPED-90° (Fig. 8) as a proxy. On the other hand, MagEIS/REPT electron phase-space distributions (PSDs) in adiabatic (μ, K, L^*) coordinates (Fig. 9) have allowed to track non-adiabatic source/loss processes along the storm (Friedel et al., 2002).

It is worth recalling here that NOAA-15/POES satellite moves along a Sun-synchronous nearly-polar LEO at an altitude of about 807 km. The on-board SEM-2 package mounts the Medium Energy Proton and Electron Detector (MEPED) (Evans & Greer, 2004), including two $\pm 15°$-wide telescopes, of which the one labeled as "90°" points a direction nearly per-

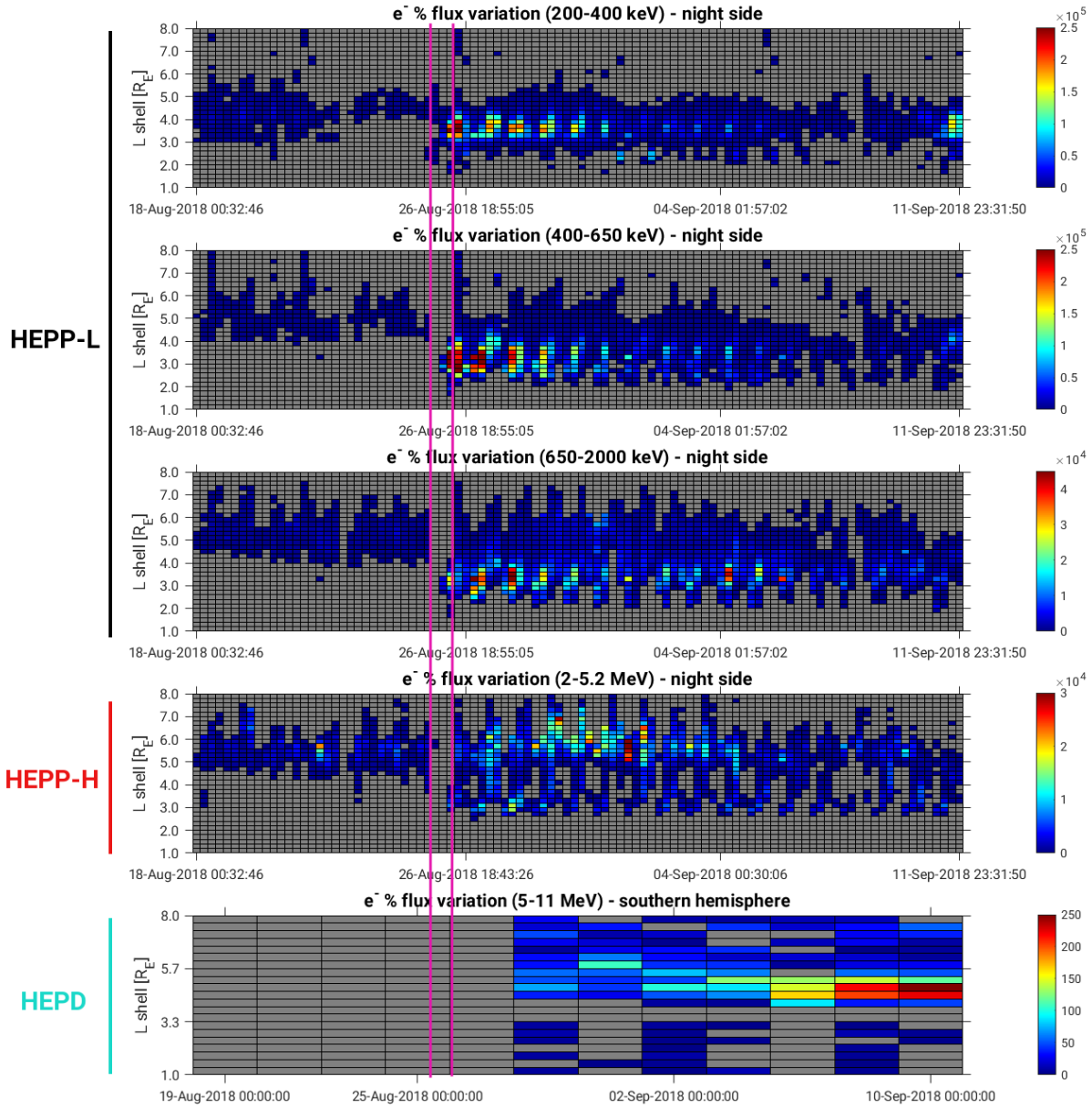

Figure 4. UTC-L maps of storm-time percent flux variations with respect to the quiet period of Aug 8-12, 2018, for: 1) electrons detected by HEPP-L in three different energy ranges (200-400 keV, 400-650 keV, and 650-2000 keV); 2) electrons detected by HEPP-H over the 2.0-5.2 MeV range; 3) electrons detected by HEPD over the 5-11 MeV range (100% counting efficiency for energies larger than $\sim$ 8 MeV; 50% at $\sim$ 5 MeV).
In any energy range, the lowest intensity bin is in gray, and full color scale is chosen in order to stress population characteristics and time evolution. Night side selection is responsible for apparent time "periodicity" of flux variations in HEPP maps. The SAA is excluded in order to skip saturation in HEPP data. HEPP-L channels that occasionally saturate also outside the SAA are excluded. Magenta lines enclosing main phase are intended as a guide for the eye.

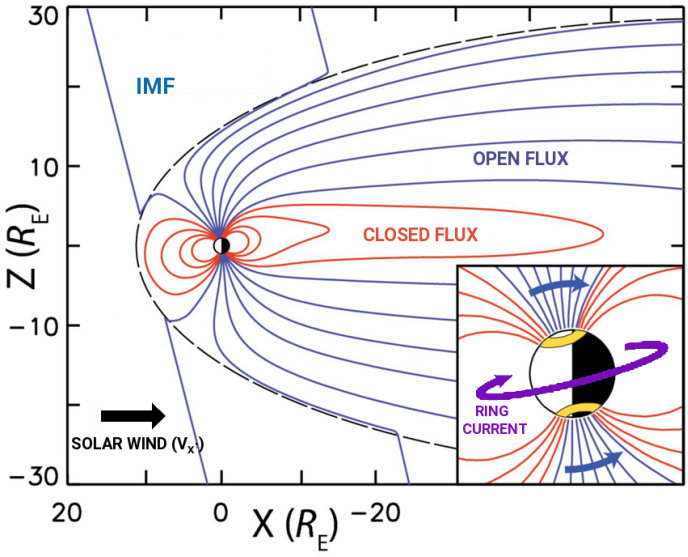

Figure 5. Schematic of the open/close magnetospheric topology produced by the Dungey cycle. The rate of day-side reconnection depends on solar wind speed and interplanetary magnetic field, while the night-side rate is controlled by magnetotail conditions. In the inset: a) the footprint of open (blue) and closed flux (red), respectively; and b) auroral ovals in yellow, encircling polar caps that undergo progressive expansion and contraction due to day-side/night-side reconnection mismatch.

Adapted from (Nichols & Milan, 2016). Figure available via license: Creative Commons Attribution 4.0 International.

pendicular to zenith and antiparallel to the spacecraft velocity (that is, in the same plane as HEPP-L/H, which is nearly orthogonal to CSES-01 velocity, though). Due to relative telescope positions and narrow field of view, at mid/high latitudes ($L > 3$) the 0° telescope mainly measures precipitation, while the 90° companion is predominantly sensitive to entrapment; this situation is roughly reversed at low latitudes (Asikainen & Mursula, 2013; Yahnin et al., 2016). Unlike the 0° device, electron channels in the 90° electron telescope are affected by small low-energy proton contamination at large L shell even in disturbed periods ($< 6.5\%$ at $L > 7$) (Rodger et al., 2010). On the other hand, the dual-spacecraft Radiation Belt Storm Probes (RBSP) mount MagEIS and REPT particle detectors (Blake et al., 2013; Baker, Kanekal, Hoxie, Batiste, et al., 2013) and, though far from a LEO mission (RBSP-A/B move along highly elliptical orbits at an inclination of 10°, with only a very fast passage in high ionosphere at the perigee), they offer an interesting point of view due to the spacecraft's direct penetration of the RBs. Background contamination is present in both MagEIS electrons and protons, due to inner zone protons and bremsstrahlung X rays, but electron measurements are subject to correction. A background (partly due to galactic cosmic rays) afflicts REPT measurements as well, especially in the highest electron channels, which induces a flattening out of the energy spectrum when the signal-to-noise ratio gets low (see `https://www.rbsp-ect.lanl.gov/science/DataQualityCaveats.php`).

5 Discussion and conclusions

The very good consistence of HEPP-L observations of sub-relativistic and relativistic ("core") electron flux variations with those by MEPED-90° and MagEIS-A along the Aug 2018 storm, as well as their coherence with expected magnetospheric flows (Fig. 5), is quite striking in spite of significant differences in either altitude or orbit inclination and shape

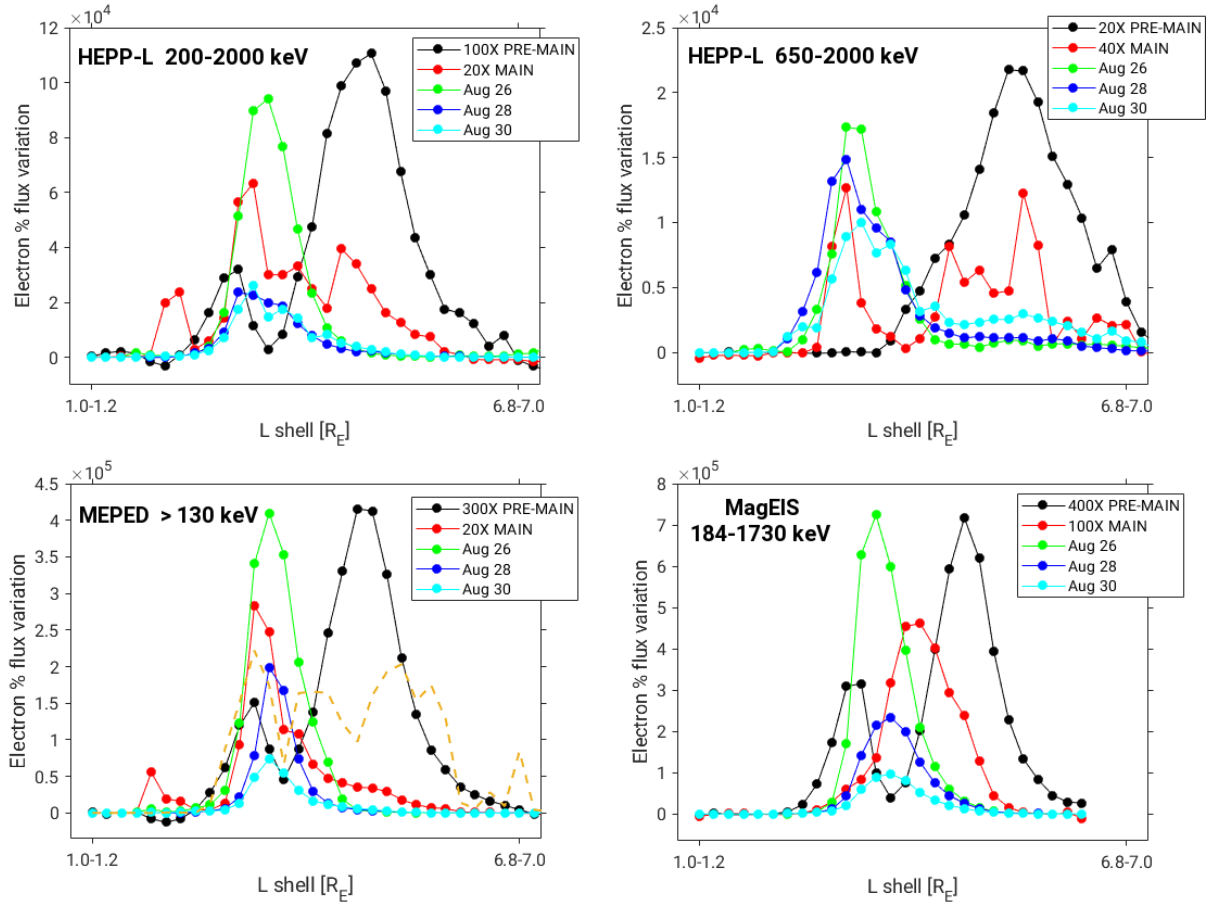

Figure 6. Synchronous observations of electron flux by different missions for the Aug 25-26, 2018 storm. Top left: night-side 1D L distributions of percent flux variations with respect to the quiet period of Aug 8-12, 2018, for 200-2000 keV electrons detected by HEPP-L during pre-main and main phase, and a triplet of days included in recovery phase. Top right: corresponding flux variations for HEPP-L 650-2000 keV electrons. Bottom left: corresponding flux variations for $>$ 130 keV electrons detected by MEPED-90° (NOAA-15/POES), with superposition of the (20X-enhanced) flux variation detected by MEPED-0° during main phase (orange dashed line). Bottom right: corresponding flux variations for 184-1730 keV electrons detected by MagEIS (RBSP-A). With the exception of MagEIS, the SAA is excluded in order to skip saturation in HEPP data. HEPP-L channels that occasionally saturate also outside the SAA are excluded.

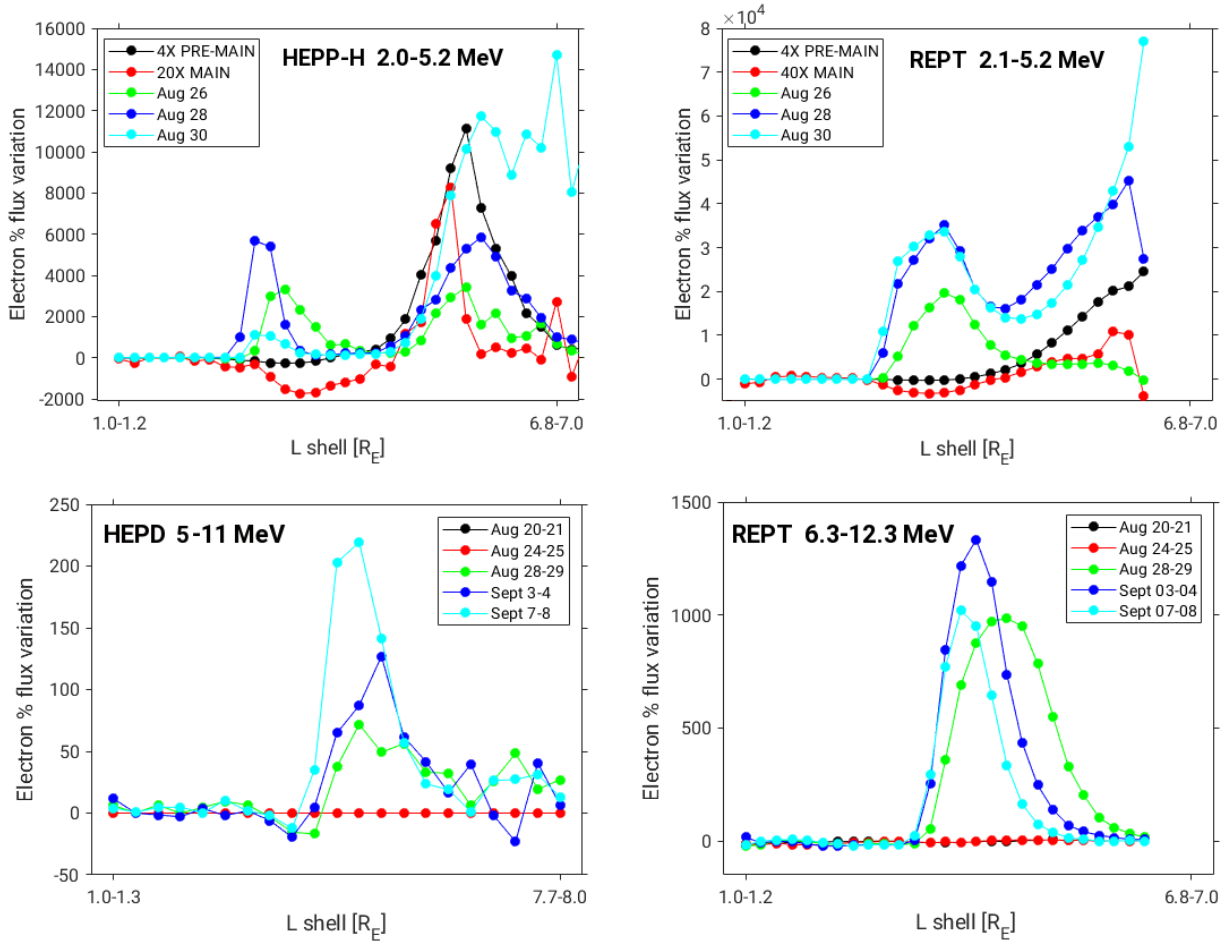

Figure 7. Synchronous observations of electron flux by different missions for the Aug 25-26, 2018 storm. Top left: night-side 1D L distributions of percent flux variations with respect to the quiet period of Aug 8-12, 2018, for 2.0-5.2 MeV electrons detected by HEPP-H during pre-main and main phase, and a triplet of days included in recovery phase. Top right: corresponding flux variations for 2.1-5.2 MeV electrons detected by REPT (RBSP-A). Bottom left: southern-hemisphere 1D L distributions of percent flux variations with respect to the quiet period of Aug 8-12, 2018, for 5-11 MeV electrons detected by HEPD (100% counting efficiency for energies larger than $\sim$ 8 MeV; 50% at $\sim$ 5 MeV) during five different 2-day intervals between filament eruption and early September. Top right: corresponding flux variations for 6.3-12.3 MeV electrons detected by REPT.
With the exception of REPT, the SAA is excluded in order to skip saturation in HEPP data.

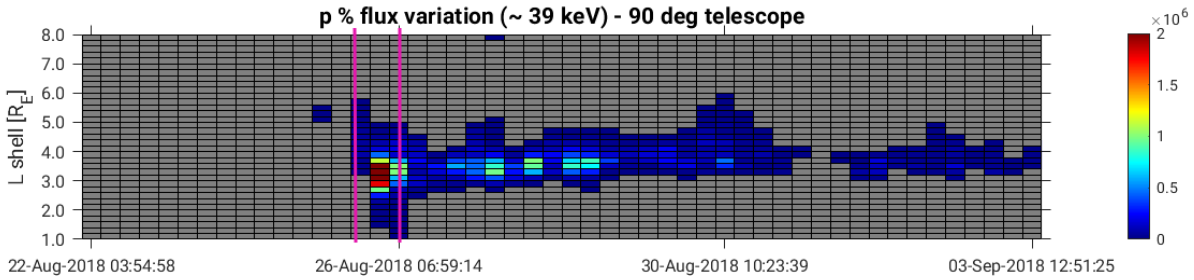

Figure 8. UTC-L map of storm-time percent flux variations with respect to the quiet period of Aug 8-12, 2018, for ∼ 39 keV protons detected by MEPED-90° (NOAA-15/POES). Time binning and L resolution are the same as those of HEPP-L/H in Fig. 4. The SAA is excluded for consistence with CSES-01 data. The lowest intensity bin is in gray. Magenta lines denote main phase of the storm.

At $L > 3$, where the detector primarily measures trapped particles, this low-energy proton dynamics can be considered as a qualitative proxy (O^+ component being neglected) of ring-current buildup and evolution in the magnetosphere, in spite of > 1 MeV electron contamination of channel P1, which remains negligible (Yahnin et al., 2016).

(Fig. 6). Prior to the impact of the ICME, magnetospheric electrons of energy < 2 MeV modestly exceed the SQ background and peak at $L \sim 3.2\ R_E$ and $\sim 4.8\ R_E$, with core populations abounding in the external portion of the ORB, as clearly shown in the top right panel of Fig. 6, where only HEPP-L electrons of energies above 650 keV are tracked along their storm-time evolution. Following the shift in L of the peaks across the storm, the compression of the magnetosphere due to the impact by the ICME, and subsequent relaxation, can be easily recognized. The main phase of the storm witnesses the emptying of the plasmasphere and an incursion of basically seed electrons into the slot (with possible precipitation, as suggested by no parallel detection by the MEPED-0° telescope, even though a detailed pitch-resolved analysis would be necessary); this latter phenomenon is captured by the two LEO missions, but not by MagEIS (transiting across its apogee at the moment when HEPP-L and MEPED start recording the event); while the relativistic counterpart is depleted at $L > 4$ by a factor ∼ 4. During recovery, a severe flux enhancement at L ∼ 3.2 R_E (up to 3 orders of magnitude) is observed with long-lasting die-off; as well as full replenishment (and even enhancement) of relativistic populations at large L shell. A partial re-energization of the outer belt can be spotted after the first week of September (Fig. 4), especially marked at lowest energies. A quick look to the shape of the top-left PSD profiles in Fig. 9 identifies a set of positive gradients for sub-relativistic electrons, which are compatible with flux enhancements triggered by radial diffusion from an external source (Green & Kivelson, 2004); the relativistic counterpart (top-right profiles in Fig. 9) shows definitely flatter, and even slightly negative, gradients in recovery, which may match the case of local acceleration.

In the relativistic range between 2 and 5 MeV, HEPP-H data (Fig. 4, fourth panel; Fig. 7, top left) show how only electrons belonging to the ORB look affected by the strong geomagnetic disturbance, with sharp inner edge at $L \sim 2.7\ R_E$ and apparent impenetrable barrier to significant inward transfer of multi-MeV particles below such edge (Baker et al., 2014, 2016). In main phase, electron fluxes undergo considerable depletion (by a factor ∼ 4 to ∼ 16) that involves the entire outer belt, and is especially marked at $L > 4$. The Dst effect, being pronounced between $L \sim 3$ and $L \sim 4$ (Fig. 8), cannot be invoked as the only cause of electron depletion. The recovery phase is characterized by an important buildup phenomenon (by two orders of magnitude), which impacts the external ORB and a narrow strip centered at $L \sim 3.2$, which progressively dies off. The features of the energized internal population are somehow reminiscent of those marking the so-called "storage ring" discovered

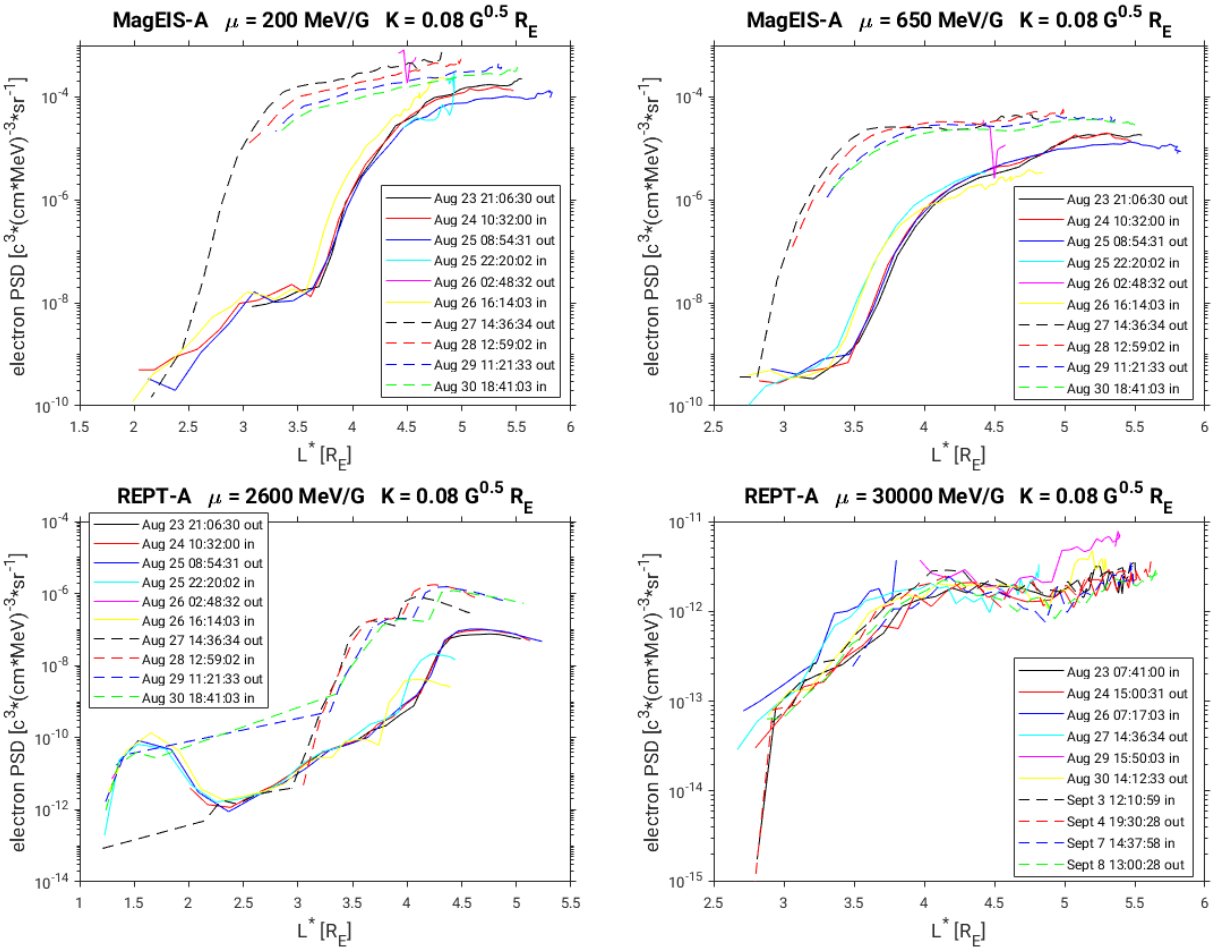

Figure 9. PSD-*vs.*-L^* profiles at costant μ and K for MagEIS/REPT-A electrons along the Aug 2018 storm. As usual, the (μ, K, L^*) coordinates correspond to the first, second, and inverse of third invariant, respectively. The four values of μ have been chosen so as to roughly match HEPP-L/H and HEPD energy ranges shown in Figs. 6-7. Details about the PSD calculation procedure - relying on the Internal Radiation Belt Environment Modeling Library (IRBEM-LIB [2004-2012]) under T04 field modeling (Tsyganenko & Sitnov, 2005) - can be found in (Hartley & Denton, 2015).

in Sept 2012 and likely resulting from losses occurring at higher L shells (Baker, Kanekal, Hoxie, Henderson, et al., 2013). The comparison to homologous measures by REPT-A (Fig. 7, right panel) is reasonably good, considering orbit differences that account for the sharp break at $L > 6.5\ R_E$ in REPT-A distributions. The related PSD profiles (Fig. 9, bottom left) are characterized by clearly negative gradients, which suggest that flux enhancements during recovery are fed by local heating.

Despite geomagnetic disturbances are much less effective on electrons of energies > 5 MeV, in the highly relativistic electron energy range monitored by HEPD, the Italian detector is able to return clear evidence for direct acceleration up to the 10-MeV order of magnitude immediately downstream of the main phase of the storm (Fig. 7, bottom left), lasting several days, peaking in the ORB around $L \sim 4.5\ R_E$, and with geographical location in the southern hemisphere (Fig. 4, last panel). Consistently, REPT-A observes an enhancement in the same L-shell range during recovery (Fig. 7, bottom right), even though with relative-intensity mismatch around Sept 7. Indeed, this inconsistency needs further investigation, since it may be accounted for invoking either orbital differences - which favor the ionospheric over the magnetospheric point of view when LEO configurations are considered - or proton contamination (currently under assessment) in the lowest bin of HEPD electron energies, or both. Also related PSD profiles (Fig. 9, bottom right) turn out extremely noisy, thus hindering proper slope assessment.

Though born with the aim to basically study the litho/iono/magnetosphere coupling in correspondence to the onset of major earthquakes, CSES-01 satellite mission has already joined successfully the challenging area of space-weather and space-climate exploration by detection of charged-particle dynamics during geomagnetic storms.

This work reports wide-energy-range data from the suite of particle detectors on board CSES-01 in relation to the G3-class geomagnetic storm that affected the Earth environment in late Aug 2018. The extended 200 keV-to-11 MeV electron energy range spanned by the combination of HEPP-L, HEPP-H and HEPD detectors has allowed for an all-around characterization of the pronounced short-term magnetospheric rearrangement in L shell in response to the solar disturbance, which has been corroborated by corresponding observations by concurrent active missions, and has turned out fairly consistent with the mainstream literature on the subject. In addition, galactic protons detected by HEPD have returned no significant storm-time dynamics, which is consistent with a solar-minimum disturbance marked by the emission of no SEPs.

Considering the sky-rocketing focus on Space Weather studies in this last decade, the above results prove promising especially in view of the planned building of a constellation of CSES satellites in the next few years, in a period when many contributors to the heterogeneous stream of missions dedicated to the monitoring of the near-Earth environment will be either quit or well beyond the end of their scheduled lifetimes.

Acknowledgments

This work makes use of data from CSES mission (`www.leos.ac.cn/`), a project funded by China National Space Administration (CNSA) and China Earthquake Administration (CEA) in collaboration with Italian Space Agency (ASI) and Istituto Nazionale di Fisica Nucleare (INFN). The Authors kindly acknowledge N. Papitashvili and J. King at the National Space Science Data Center of the Goddard Space Flight Center for the use permission of 1-hr OMNI data, and the NASA CDAWeb team for making these data available. They also acknowledge use of NOAA Space Weather Prediction Center for obtaining GOES-15 proton fluxes; as well as NOAA National Geophysical Data Center (`https://ngdc.noaa.gov/ngdc.html`) for MEPED electron fluxes from NOAA-15/POES. Still, they acknowledge the NMDB database (`www.nmdb.eu`), founded under the European Union's

FP7 programme (contract no. 213007) for providing neutron-monitor data: specifically, Terre Adelie (TERA) data were kindly provided by the Observatoire de Paris and French polar institute (IPEV), France. Finally, the Authors acknowledge the RBSP-ECT Science Operations and Data Center (`https://www.rbsp-ect.lanl.gov/rbsp_ect.php`, and `https://rbspgway.jhuapl.edu`) for use and analysis of MagEIS-A and REPT-A electron data.

This work was supported by ASI in the framework of the Accordo Attuativo no. 2016-16-H0 Progetto Limadou Fase E/Scienza (CUP F12F1600011005).

References

Adriani, O., Barbarino, G. C., Bazilevskaya, G. A., Bellotti, R., Boezio, M., Bogomolov, E. A., ... others (2015). Pamela's Measurements of Magnetospheric Effects on High Energy Solar Particles. *Astrophys. J. Lett.*, *801*(1), L3. doi: 10.1088/2041-8205/801/1/L3

Adriani, O., Barbarino, G. C., Bazilevskaya, G. A., Bellotti, R., Boezio, M., Bogomolov, E. A., ... others (2016). PAMELA's Measurements of Geomagnetic Cutoff Variations during the 14 December 2006 Storm. *Space Weather*, *14*, 210-220. doi: 10.1002/2016SW001364

Ambrosi, G., Bartocci, S., Basara, L., Battiston, R., J., B. W., Campana, D., ... others (2020). Beam Test Calibrations of the HEPD Detector on board the China Seismo-Electromagnetic Satellite. *Nucl. Instrum. Meth. A*, *974*, 164170. doi: 10.1016/j.nima.2020.164170

Andriopoulou, M., Mavromichalaki, H., Plainaki, C., Belov, A., & Eroshenko, E. (2011). Intense Ground-Level Enhancements of Solar Cosmic Rays During the Last Solar Cycles. *Sol. Phys.*, *269*(1), 155-168. doi: 10.1007/s11207-010-9678-1

Asikainen, T., & Mursula, K. (2013). Correcting the NOAA/MEPED Energetic Electron Fluxes for Detector Efficiency and Proton Contamination. *J. Geophys. Res. Space Phys.*, *118*, 6500-6510. doi: 10.1002/jgra.50584

Asvestari, E., Willamo, T., Gil, A., Usoskin, I. G., Kovaltsov, G. A., Mikhailov, V. V., & Mayorov, A. (2017). Analysis of Ground Level Enhancements (GLE): Extreme Solar Energetic Particle Events have Hard Spectra. *Advan. Space Res.*, *60*(4), 781-787. doi: 10.1016/j.asr.2016.08.043

Baker, D. N., Hoxie, V., Zhao, H., Jaynes, A. N., Kanekal, S., Li, X., & Elkington, S. (2019). Multiyear Measurements of Radiation Belt Electrons: Acceleration, Transport, and Loss. *J. Geophys. Res. Space Phys.*, *124*, 2588-2602. doi: 10.1029/2018JA026259

Baker, D. N., Jaynes, A. N., Hoxie, V. C., Thorne, R. M., Foster, J. C., Li, X., ... others (2014). An Impenetrable Barrier to Ultrarelativistic Electrons in the Van Allen Radiation Belts. *Nature*, *515*, 531-534. doi: 10.1038/nature13956

Baker, D. N., Jaynes, A. N., Kanekal, S., Foster, J. C., Erickson, P. J., Fennel, J. F., ... others (2016). Highly Relativistic Radiation Belt Electron Acceleration, Transport, and Loss: Large Solar Storm Events of March and June 2015. *J. Geophys. Res. Space Phys.*, *121*, 6647-6660. doi: 10.1002/2016JA022502

Baker, D. N., Kanekal, S. G., Hoxie, V., Batiste, S. N., Bolton, M., Li, X., ... others (2013). The Relativistic Electron-Proton Telescope (REPT) Instrument on board the Radiation Belt Storm Probes (RBSP) Spacecraft: Characterization of Earth's Radiation Belt High-Energy Particle Populations. *Space Sci. Rev.*, *179*, 337–381. doi: 10.1007/s11214-012-9950-9

Baker, D. N., Kanekal, S. G., Hoxie, V. C., Henderson, M. G., Li, X., Spence, H. E., ... others (2013). A Long-Lived Relativistic Electron Storage Ring Embedded in Earth's Outer Van Allen Belt. *Science*, *340*(6129), 186-190. doi: 10.1126/science.1233518

Blake, J. B., Carranza, P. A., Claudepierre, S. G., Clemmons, J. H., Crain Jr, W. R., Dotan, Y., ... others (2013). The Magnetic Electron Ion Spectrometer (MagEIS) Instruments aboard the Radiation Belt Storm Probes (RBSP) Spacecraft. *Space Sci.*

Rev., *179*(1-4), 383–421. doi: 10.1007/s11214-013-9991-8

Claudepierre, S. G., Elkington, S. R., & Wiltberger, M. (2008). Solar Wind Driving of Magnetospheric ULF Waves: Pulsations Driven by Velocity Shear at the Magnetopause. *J. Geophys. Res. Space Phys.*, *113*(A5). doi: 10.1029/2007JA012890

Dietze, G., Bartlett, D. T., Cool, D. A., Cucinotta, F. A., Jia, X., McAulay, I. R., ... others (2013). Icrp publication 123. assessment of radiation exposure of astronauts in space. *Ann. ICRP*, *42*(4), 1-339. doi: 10.1016/j.icrp.2013.05.004

Dungey, J. W. (1961). Interplanetary Magnetic Fields and the Auroral Zones. *Phys. Rev. Lett.*, *6*, 47-48. doi: 10.1103/PhysRevLett.6.47

Eastwood, J., Hapgood, M. A., Biffis, E., Benedetti, D., Bisi, M. M., Green, L., ... Burnett, C. (2018). Quantifying the Economic Value of Space Weather Forecasting for Power Grids: An Exploratory Study. *Space Weather*, *16*(12), 2052-2067. doi: 10.1029/2018SW002003

Evans, D. S., & Greer, M. S. (2004). Polar Orbiting Environmental Satellite Space Environment Monitor–2 Instrument Descriptions and Archive Data Documentation. *NOAA Tech. Mem. 1.4, Space Environ. Lab., Boulder, Colorado*.

Fennell, J. F., Claudepierre, S. G., Blake, J. B., O'Brien, T. P., Clemmons, J. H., Baker, D. N., ... Reeves, G. D. (2015). Van Allen Probes Show that the Inner Radiation Zone Contains no MeV Electrons: ECT/MagEIS Data. *Geophys. Res. Lett.*, *42*, 1283-1289. doi: 10.1002/2014GL062874

Foster, J. C., Erickson, P. J., Baker, D. N., Claudepierre, S. G., Kletzing, C. A., Kurth, W., ... others (2014). Prompt Energization of Relativistic and Highly Relativistic Electrons during a Substorm Interval: Van Allen Probes Observations. *Geophys. Res. Lett.*, *41*, 20-25. doi: 10.1002/2013GL058438

Friedel, R. H. W., Reeves, G. D., & Obara, T. (2002). Relativistic electron dynamics in the inner magnetosphere - a review. *J. Atmos. Sol.-Terr. Phys.*, *64*, 265-282. doi: 10.1016/S1364-6826(01)00088-8

Ganushkina, N., Jaynes, A., & Liemohn, M. (2017). Space Weather Effects Produced by the Ring Current Particles. *Space Sci. Rev.*, *212*, 1315-1344. doi: 10.1007/s11214-017-0412-2

Goldstein, J., Baker, D. N., Blake, J. B., De Pascuale, S., Funsten, H. O., Jaynes, A. N., ... others (2016). The relationship between the plasmapause and outer belt electrons. *J. Geophys. Res. Space Phys.*, *121*, 8392-8416. doi: 10.1002/2016JA023046

Green, J. C., & Kivelson, M. G. (2004). Relativistic Electrons in the Outer Radiation Belt: Differentiating between Acceleration Mechanisms. *J. Geophys. Res.*, *109*, A03213. doi: 10.1029/2003JA010153

Hale, G. E., Ellerman, F., Nicholson, S. B., & Joy, A. H. (1919). The Magnetic Polarity of Sun-Spots. *Astrophys. J.*, *49*, 153. doi: 10.1086/142452

Hartley, D. P., & Denton, M. H. (2015). Solving the Radiation Belt Riddle. *A&G*, *55*(6), 6.17-6.20. doi: 10.1093/astrogeo/atu247

Iju, T., Tokumaru, M., & Fujiki, K. (2013). Radial Speed Evolution of Interplanetary Coronal Mass Ejections during Solar Cycle 23. *Sol. Phys.*, *288*, 331-353. doi: 10.1007/s11207-013-0297-5

James, M. K., Yeoman, T. K., Mager, P. N., & Klimushkin, D. Y. (2013). The Spatio-Temporal Characteristics of ULF Waves Driven by Substorm Injected Particles. *J. Geophys. Res. Space Phys.*, *118*(4), 1737-1749. doi: 10.1002/jgra.50131

Jaynes, A. N., Baker, D. N., Singer, H. J., Rodriguez, J. V., Lotoaniu, T. M., Ali, A. F., ... others (2015). Source and Seed Populations for Relativistic Electrons: Their Roles in Radiation Belt Changes. *J. Geophys. Res. Space Phys.*, *120*, 7240-7254. doi: 10.1002/2015JA021234

Katsavrias, C., Sandberg, I., Li, W., Podladchikova, O., Daglis, I. A., Papadimitriou, C., ... Aminalragia-Giamini, S. (2019). Highly Relativistic Electron Flux Enhancement During the Weak Geomagnetic Storm of April–May 2017. *J. Geophys. Res. Space Phys.*, *124*(6), 4402-4413. doi: 10.1029/2019JA026743

Kauristie, K., Morschhauser, A., Olsen, N., Finlay, C. C., McPherron, R. L., Gjerloev, J. W.,

& Opgenoorth, H. J. (2017). On the Usage of Geomagnetic Indices for Data Selection in Internal Field Modelling. *Space Sci. Rev.*, *206*, 61-90. doi: 10.1007/s11214-016-0301-0

Kay, C., Airapetian, V. S., Lueftinger, T., & Kochukhov, O. (2019). Frequency of Coronal Mass Ejection Impacts with Early Terrestrial Planets and Exoplanets around Active Solar-like Stars. *Astrophys. J. Lett.*, *886*(2), L37. doi: 10.3847/2041-8213/ab551f

Keika, K., Kistler, L. M., & Brandt, P. C. (2013). Energization of O^+ Ions in the Earth's Inner Magnetosphere and the Effects on Ring Current Buildup: A Review of Previous Observations and Possible Mechanisms. *J. Geophys. Res. Space Phys.*, *118*, 4441–4464. doi: 10.1002/jgra.50371

Li, X.-Q., Xu, Y.-B., Z-H., A., Liang, X.-H., Wang, P., Zhao, X.-Y., ... others (2019). The High-Energy Particle Package on board CSES. *Radiat. Detect. Technol. Methods*, *3*, 22. doi: 10.1007/s41605-019-0101-7

Lyons, L. R., Thorne, R. M., & Kennel, C. F. (1972). Pitch-Angle Diffusion of Radiation Belt Electrons Within the Plasmasphere. *J. Geophys. Res.*, *77*(19), 3455-3474. doi: 10.1029/JA077i019p03455

Ma, Q., Li, W., Thorne, R. M., Bortnik, J., Reeves, G. D., Spence, H. E., ... others (2017). Diffusive Transport of Several Hundred keV Electrons in the Earth's Slot Region. *J. Geophys. Res. Space Phys.*, *122*, 10235-10246. doi: 10.1002/2017JA024452

McIlwain, C. E. (1966). Ring Current Effects on Trapped Particles. *J. Geophys. Res.*, *71*, 3623-3628. doi: 10.1029/JZ071i015p03623

Nichols, J. D., & Milan, S. (2016). Stellar Wind-Magnetosphere Interaction at Exoplanets: Computations of Auroral Radio Powers. *Mon. Not. R. Astron. Soc.*, *461*(3), 2353-2366. doi: 10.1093/mnras/stw1430

Pesnell, W. D. (2008). Predictions of Solar Cycle 24. *Solar Phys.*, *252*, 209-220. doi: 10.1007/s11207-008-9252-2

Picozza, P., Battiston, R., Ambrosi, G., Bartocci, S., Basara, W. J., L. abd Burger, Campana, D., et al. (2019). Scientific Goals and In-Orbit Performance of the High-Energy Particle Detector on board the CSES. *ApJS*, *243*, 16. doi: 10.3847/1538-4365/ab276c

Piersanti, M. (2019). The August 2018 Geomagnetic Storm: A Multi-Instrumental Analysis from CSES Analysis and Ground Magnetometers. *The 1st International Symposium on Geo-hazards Perception, Cognition and Prediction (PCP) & The 4th International Workshop of CSES Mission, Beijing*. doi: 10.13140/RG.2.2.26117.50400

Piersanti, M., Alberti, T., Bemporad, A., Berrilli, F., Bruno, R., Capparelli, V., ... others (2017). Comprehensive Analysis of the Geoeffective Solar Event of 21 June 2015: Effects on the Magnetosphere, Plasmasphere, and Ionosphere Systems. *Solar Physics*, *292*(11), 169. doi: 10.1007/s11207-017-1186-0

Piersanti, M., & Carter, B. A. (2019). *Geomagnetically Induced Currents, in The Dynamical Ionosphere. A Systems Approach to Ionospheric Irregularity* (M. Materassi, B. Forte, A. Coster, & S. Skone, Eds.). Elsevier.

Piersanti, M., Villante, U., Waters, C., & Coco, I. (2012). The 8 June 2000 ULF Wave Activity: A Case Study. *J. Geophys. Res.*, *117*, A02204. doi: 10.1029/2011JA016857

Reeves, G. D., Friedel, R. H. W., Larse, B. A., Skoug, R. M., Funsten, H. O., Claudepierre, S. G., ... others (2016). Energy-dependent dynamics of kev to mev electrons in the inner zone, outer zone, and slot regions. *J. Geophys. Res. Space Phys.*, *121*, 397–412. doi: 10.1002/2015JA021569

Rodger, C. J., Clilverd, M. A., Green, J. C., & Lam, M. M. (2010). Use of POES SEM-2 Observations to Examine Radiation Belt Dynamics and Energetic Electron Precipitation into the Atmosphere. *J. Geophys. Res.*, *115*, A04202. doi: 10.1029/2008JA014023

Schrijver, C. J., Kauristie, K., Aylward, A. D., Denardini, C. M., Gibson, S. E., Glover, A., ... others (2015). Understanding Space Weather to Shield Society: A Global Road Map for 2015–2025 Commissioned by COSPAR and ILWS. *Adv. Space Res.*, *55*, 2745-2807. doi: 10.1016/j.asr.2015.03.023

Schulz, M., & Lanzerotti, L. J. (1974). *Particle Diffusion in the Radiation Belts*. Berlin: Springer.

Selesnick, R. S., Looper, M. D., & Mewaldt, R. A. (2007). A Theoretical Model of the Inner

Proton Radiation Belt. *Space Weather*, *5*(4). doi: 10.1029/2006SW000275

Shen, X.-H., Zhang, X.-M., Yuan, S.-G., Wang, L.-W., Cao, J.-B., Huang, J.-P., ... Dai, J.-P. (2018). The State-of-the-art of the China Seismo-Electromagnetic Satellite Mission. *Sci. China Technol. Sci.*, *61*(5), 634-642. doi: 10.1007/s11431-018-9242-0

Thébault, E., Finlay, C. C., Beggan, C. D., Alken, P., Aubert, J., Barrois, O., ... others (2015). International Geomagnetic Reference Field: the 12th Generation. , *67*(79). doi: 10.1186/s40623-015-0228-9

Thorne, R. M., Li, W., Ni, B., Ma, Q., Bortnik, J., Chen, L., ... others (2013). Rapid Local Acceleration of Relativistic Radiation-Belt Electrons by Magnetospheric Chorus. *Nature*, *504*, 411-414. doi: 10.1038/nature12889

Tsyganenko, N. A., & Sitnov, M. I. (2005). Modeling the Dynamics of the Inner Magnetosphere during Strong Geomagnetic Storms. *J. Geophys. Res.*, *110*(A3). doi: 10.1029/2004JA010798

Turner, D. L., Kilpua, E. K. J., Hietala, H., Claudepierre, S. G., O'Brien, T. P., Fennell, J. F., ... others (2019). The Response of Earth's Electron Radiation Belts to Geomagnetic Storms: Statistics From the Van Allen Probes Era Including Effects From Different Storm Drivers. *J. Geophys. Res. Space Phys.*, *124*, 1013-1034. doi: 10.1029/2018JA026066

Turner, D. L., O'Brien, T. P., Fennel, J. F., Claudepierre, S. G., Blake, J. B., Kilpua, E. K. J., & Hietala, H. (2015). The effects of geomagnetic storms on electrons in earth's radiation belts. *Geophys. Res. Lett.*, *42*, 9176-9184. doi: 10.1002/2015GL064747

Turner, D. L., O'Brien, T. P., Fennell, J. F., Claudepierre, S. G., Blake, J. B., Jaynes, A. N., ... others (2017). Investigating the Source of Near-Relativistic and Relativistic Electrons in Earth's Inner Radiation Belt. *J. Geophys. Res. Space Phys.*, *122*, 695-710. doi: 10.1002/2016JA023600

Turner, D. L., Shprits, Y., Hartinger, M., & Angelopoulos, V. (2012). Explaining Sudden Losses of Outer Radiation Belt Electrons During Geomagnetic Storms. *Nature Physics*, *8*, 208-212. doi: 10.1038/NPHYS2185

Ukhorskiy, A. Y., Sitnov, M. I., Millan, R. M., Kress, B. T., Fennell, J. F., Claudepierre, S. G., & Barnes, R. J. (2015). Global Storm Time Depletion of the Outer Electron Belt. *J. Geophys. Res. Space Phys.*, *120*(4), 2543–2556. doi: 10.1002/2014JA020645

Yahnin, A. G., Yahnina, T. A., Semenova, N. V., Gvozdevsky, B. B., & Pashin, A. B. (2016). Relativistic Electron Precipitation as Seen by NOAA POES. *J. Geophys. Res. Space Phys.*, *121*, 8286-8299. doi: 10.1002/2016JA022765

Yan, R., Shen, X.-H., Huang, J.-P., Wang, Q., Chu, W., Liu, D.-P., ... others (2018). Examples of Unusual Ionospheric Observations by the CSES prior to Earthquakes. *Earth Planet. Phys.*, *2*(6), 515-526. doi: 10.26464/epp2018050

Zhang, X.-M., Frolov, V., Zhao, S.-F., Zhou, C., Wang, Y.-L., Ryabov, A., & Zhai, D.-L. (2018). The First Joint Experimental Results between SURA and CSES. *Earth Planet. Phys.*, *2*(6), 527-537. doi: 10.26464/epp2018051

Zhao, H., Baker, D. N., Jaynes, A. N., & Kanekal, S. G. (2019). The Effects of Geomagnetic Storms and Solar Wind Conditions on the Ultrarelativistic Electron Flux Enhancements. *J. Geophys. Res. Space Phys.*, *124*(3), 1948-1965. doi: 10.1029/2018JA026257

Zong, Q.-J., Zhou, X.-Z., Wang, Y.-F., Li, X., Song, P., Baker, D. N., ... others (2009). Energetic Electron Response to ULF Waves Induced by Interplanetary Shocks in the Outer Radiation Belt. *J. Geophys. Res. Space Phys.*, *114*(A10). doi: 10.1029/2009JA014393